

OPTIMISATION OF THE CATHODE COMPOSITION FOR THE INTERMEDIATE TEMPERATURE SOFC

Enn Lust, Priit Möller, Indrek Kivi, Gunnar Nurk, Silvar Kallip,
Priit Nigu, Karmen Lust
Institute of Physical Chemistry, Univ. of Tartu, Jakobi 2, 51014 Tartu, Estonia

ABSTRACT

Electrochemical characteristics of the half-cells $\text{Ce}_{0.8}\text{Gd}_{0.2}\text{O}_{1.9} \mid \text{La}_{0.6}\text{Sr}_{0.4}\text{CoO}_{3-\delta}$ (Sys 1), $\text{Ce}_{0.8}\text{Gd}_{0.2}\text{O}_{1.9} \mid \text{Pr}_{0.6}\text{Sr}_{0.4}\text{CoO}_{3-\delta}$ (Sys 2) and $\text{Ce}_{0.8}\text{Gd}_{0.2}\text{O}_{1.9} \mid \text{Gd}_{0.6}\text{Sr}_{0.4}\text{CoO}_{3-\delta}$ (Sys 3) have been studied by electrochemical impedance, cyclic voltammetry and chronoamperometry methods at various electrode potentials ΔE and temperatures T . The analysis of Z' , Z'' -plots shows that at lower temperature the kinetically mixed process is probable, characterised by the slow electron transfer to an adsorbed and thereafter dissociated oxygen atom O_{ads} as well as by slow mass transfer (i.e. diffusion-like process) of electroactive species inside the cathode or O_{ads} at the internal surface of the porous cathode. The total polarisation resistance increases in the order $\text{Sys 1} < \text{Sys 2} < \text{Sys 3}$, i.e. with rising the atom mass of the A site cation in the porous perovskite structure. The activation energy, obtained from the Arrhenius-like plots, has been found to decrease slightly with increasing negative polarisation and in the order of half-cells $\text{Sys 3} > \text{Sys 2} > \text{Sys 1}$. The transfer coefficient for the total oxygen reduction reaction $\alpha_c > 0.5$ dependent on the half-cell studied has been obtained from the Tafel-like overvoltage versus current density plots, indicating the deviation of the mainly charge transfer limited process toward the mass transfer limited process (Sys 2 and Sys 3) in the porous cathode with decreasing temperature. The electrochemical behaviour of half-cells Sys 2 and Sys 1 has been tested during long operation times $t \leq 1200$ hours.

INTRODUCTION

Solid oxide fuel cells (SOFCs) operating at intermediate temperatures become of great interest as a potential commercial clean and efficient means of co-producing electricity and heat in a variety of commercial and industrial applications (1-7). The electrochemical properties of interfaces between porous $\text{La}_{0.6}\text{Sr}_{0.4}\text{CoO}_{3-\delta}$ (LSCO) and B-site substituted $\text{La}_{1-x}\text{Sr}_x\text{Co}_{1-y}\text{Fe}_y\text{O}_{3-\delta}$ (LSCFO) as well as mixed with various electrolytes LSCO, for example $\text{La}_{0.6}\text{Sr}_{0.4}\text{Co}_{0.2}\text{Fe}_{0.8}\text{O}_{3-\delta} + \text{Ce}_{0.9}\text{Gd}_{0.1}\text{O}_{2-\delta}$ cathode and $\text{Ce}_{0.8}\text{Gd}_{0.2}\text{O}_{1.9}$ (CGO) electrolyte at intermediate temperatures (500...700°C) has been investigated (4-7) using impedance spectroscopy (IS), cyclic voltammetry (CV), secondary ion mass spectrometry (SIMS), thermogravimetry (TG) etc. methods. The optimum CGO addition equal to 30% by weight to the LSCFO fractional cathode material resulted in four times lower area specific resistivity, but the electrochemical properties of these composites

were found to be quite sensitive to the microstructure and composition of the cathode (4). Several promising cathode materials have been selected out but it was found that the electrochemical parameters are very sensitive to the method used for the preparation of the cathode as well as electrolyte. Influence of the chemical nature of the atoms positioned into the perovskite A-site is an open question (1-20). The good ionic and electronic conductivities were obtained for $\text{Pr}_{1-x}\text{Sr}_x\text{CoO}_{3-\delta}$ (PSCO) and $\text{Gd}_{1-x}\text{Sr}_x\text{CoO}_{3-\delta}$ (GSCO), however, there are no experimental data obtained during long operation times as well as under the conditions of repetitive thermocycling (9-12). The maximum electrical conductivity for PSCO has been obtained at $x = 0.4$, and introduction of the Sr^{2+} cations into the A-site of the orthorhombic perovskite lattice (Pb nm space group) is compensated by oxidation of Co^{3+} to Co^{4+} (holes) at $x \leq 0.15$ and by formation of the oxygen vacancies even at room temperature, if $x \geq 0.4$. At $293 < T < 773$ for $x \leq 0.4$ (the formation of vacancies is not significant), the linear thermal expansion coefficient (TEC) generally increases with x according to the Grüneisen's law (14).

$$\alpha_V = \frac{\gamma_G C_V \chi}{V} \quad [1]$$

where α_V is the volume TEC, γ_G is the Grüneisen's constant, C_V is the heat capacitance at constant volume, χ is the compressibility and V is the volume. As the Sr content increases, the unit cell volume also increases and as a result the TEC is expected to decrease in agreement with experimental results (15). A semimetallic behaviour is noticed for $\text{Pr}_{1-x}\text{Sr}_x\text{CoO}_{3-\delta}$ if temperature exceeds 773 K and x varies from 0.15 to 0.4. Goodenough et al. (16,17) and Bhide et al. (18) investigated the lanthanum cobaltite system and explained its conductivity behaviour in terms of the spin state of the cobalt ions. They found that the diamagnetic low-spin Co^{3+} ($t_{2g}^6 e_g^0$) exists at low temperature, while it transforms to the high-spin Co^{3+} ($t_{2g}^4 e_g^2$) with increasing temperature, due to the small energy difference between two states.

According to Rossignol et al. (19), $\text{Pr}_{0.5}\text{Sr}_{0.5}\text{CoO}_{3-\delta}$ (PSCO) and $\text{Gd}_{0.5}\text{Sr}_{0.5}\text{CoO}_{3-\delta}$ (GSCO) show the best performance on the $\text{Ce}_{1-x}\text{Gd}_x\text{O}_{3-\delta}$ (CGO) electrolyte, achieving an area specific resistance (ASR) between 0.1 and 0.2 $\Omega \text{ cm}^2$ at 650°C. At $T < 923$ K, the values of ASR are very high. The PSCO | bilayered CGO | YSZ electrolyte systems show ASR equal to 0.2 $\Omega \text{ cm}^2$ at $T = 1023$ K and ASR = 0.3 $\Omega \text{ cm}^2$ at $T = 973$ K. Long-term testing results show the stable ASR values for 500 hours at $T = 1073$ K. Thermal cycling between room temperature and 1073 K after long-term testing show minimal degradation (20).

$\text{Gd}_{0.8}\text{Sr}_{0.2}\text{CoO}_{3-\delta}$ crystallises into the orthorhombic system and the electrical conductivity is $\sim 100 \text{ S cm}^{-1}$ at $T = 1000$ K. Cathodic polarisation tests show comparatively low oxygen reduction overpotentials at the current density $i_c = 0.1 \text{ A cm}^{-2}$ in comparison with Mn-rich cathodes (21,22). Mn-rich $\text{Gd}_{1-x}\text{Sr}_x\text{Co}_{1-y}\text{Mn}_y\text{O}_{3-\delta}$ cathodes ($y = 0.2$) prepared at 8 mol% yttria-stabilised zirconia (YSZ) show thermal expansion compatibility with YSZ and only small amounts of unstable pyrochlore phase $\text{Gd}_2\text{Zr}_2\text{O}_7$ formed at 1273 K dissolve into the YSZ lattice at temperatures higher than 1000°C (21). SrZrO_2 formation has been noted at lower T for high Co-containing compositions, with reaction occurring

at higher temperatures for compositions containing even less Co (21). Thus, $\text{Gd}_{1-x}\text{Sr}_x\text{Co}_{1-y}\text{Mn}_y\text{O}_{3-\delta}$ | YSZ system can not be used for preparation of the long-lasting SOFCs (22).

It is widely accepted (1, 2, 4, 7) that there are actually three macroscopic pathways available for O_2 reduction process to occur on porous cathode | solid electrolyte structures and kinetics of this reaction is influenced by several factors: (a) the reaction of molecular oxygen with CGO electrolyte surface can be neglected at low temperatures as the surface exchange coefficient is very low (4); (b) dissociative adsorption of oxygen molecules followed by surface diffusion toward the three-phase boundary (TPB); and (c) surface reaction followed by dissolution (adsorption/absorption) of charged oxygen species in the cathode and diffusion of oxygen ions toward the cathode | electrolyte boundary can be the rate-determining steps. The solid state mass transfer of oxygen ions includes normal bulk lattice diffusion together with contribution from the grain boundary and dislocation core pathways depending on the level of bulk diffusivity.

The main aim of this work was to obtain the gas phase characteristics (using BET gas adsorption (absorption) measurement method) and electrochemical characteristics of the half-cells with various cathode and electrolyte compositions during long operation times under the conditions of cathodic polarisation and thermocycling.

EXPERIMENTAL DETAILS AND HALF-CELLS PREPARATION

The $\text{La}_{0.6}\text{Sr}_{0.4}\text{CoO}_{3-\delta}$ (LSCO) cathode and $\text{Ce}_{0.8}\text{Gd}_{0.2}\text{O}_{1.9-\delta}$ (CGO) electrolyte materials have been prepared according to Ref. (3). $\text{Pr}_{0.6}\text{Sr}_{0.4}\text{CoO}_{3-\delta}$ (PSCO) and $\text{Gd}_{0.6}\text{Sr}_{0.4}\text{CoO}_{3-\delta}$ (GSCO) have been synthesised from Pr_6O_{11} (99.9 %) and Gd_2O_3 (99.9 %), SrCO_3 and Co_2O_3 by usual solid state reaction during heating for 25 hours at $T = 1473$ K. The single phase LSCO, PSCO and GSCO materials formed were crushed and ball-milled in ethanol and, after adding an organic binder, were screenprinted on one side of the CGO electrolyte as a cathode (working electrode) and sintered at $T = 1323$ K for 5 hours. The Pt-paste (Engelhard) has been used for preparation of the very porous Pt-counter and Luggin-like reference electrodes (Pt | porous Pt | oxygen) (3). The BET adsorption, X-ray diffraction, scanning electron microscopy, STM and AFM methods have been used for the analysis of materials prepared. The following BET specific surface areas: 14; 7; and $6 \text{ m}^2 \text{ g}^{-1}$ have been obtained for Sys 1, Sys 2 and Sys 3, respectively. According to the BET and AFM data, there are micro- (nano-), meso-, and macro- (transport) pores inside the cathode materials.

EXPERIMENTAL RESULTS

Nyquist plots

Comparison of Nyquist plots (Fig. 1) for systems investigated indicates that the shape of impedance spectra noticeably depends on the chemical composition of the cathode studied. Differently from Sys 1, for Sys 2 and Sys 3 there is only one very well exposed semicircle in the Z' , Z'' -plots at $f < 2$ kHz in the whole temperature region studied ($723 \leq$

$T \leq 973$ K). However, there are deviations from the semicircle in the Z'' , Z' -plots at $1 < f < 20$ kHz. The existence of two semicircles in the Z'' , Z' -plots for Sys 1 indicates the possibility of two separate reduction processes with comparatively different time constants ($\tau_{\max} = (2\pi f_{\max})^{-1}$) obtained from the maximum frequency f_{\max} in the Z'' , Z' -plots. At higher frequencies ($f > 50$ kHz) the additional third semicircle in the case of Sys 1 and second semicircle for Sys 2 and Sys 3 have been established, characterising the grain-boundary response. Sometimes a capacitive behaviour can be observed even at very high frequencies $f > 1 \times 10^6$ Hz and these parts of the impedance spectra characterise the bulk properties of the electrode (mainly electrolyte) materials (3, 4, 7). Usually, the very high frequency (i.e. so-called bulk) semicircles are incomplete because the time constant of the bulk electrolyte response is too short even at $T \leq 773$ K.

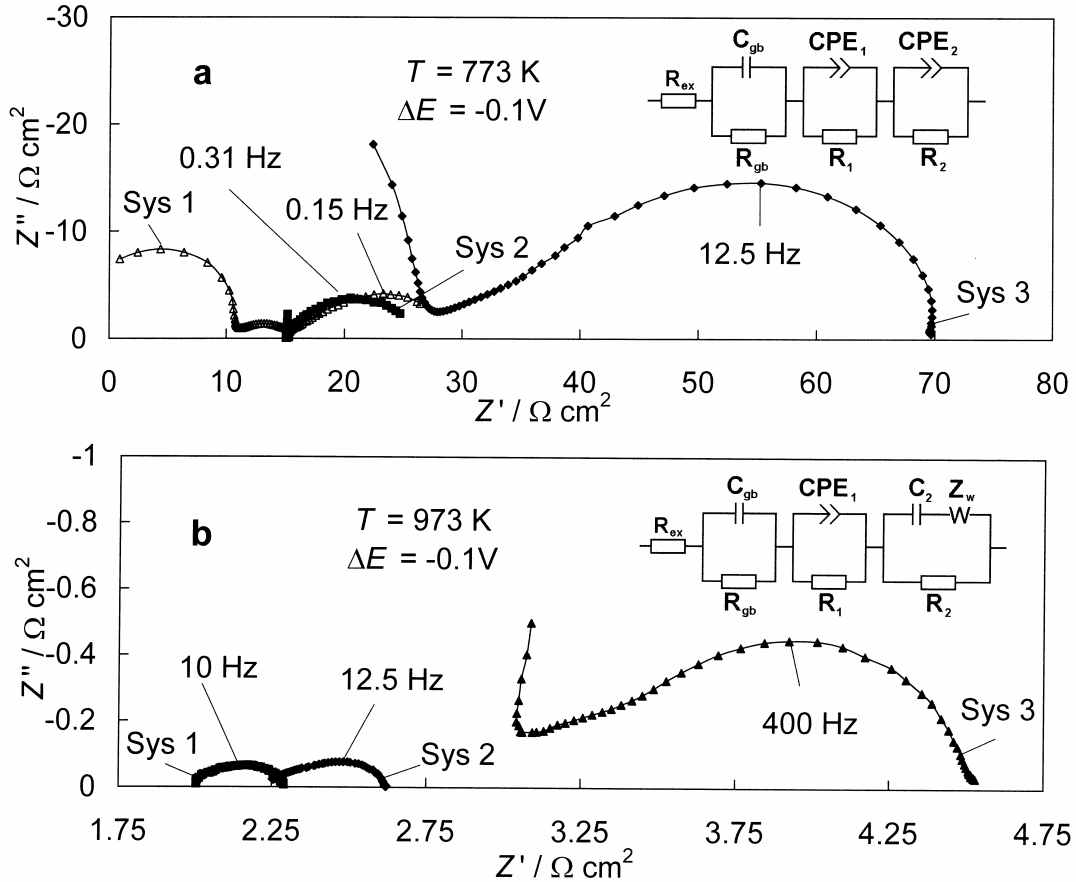


Figure 1. Nyquist plots for systems studied.

Three parameters can be obtained for each arc: the resistance R (from the intercept on the Z' -axis), the capacitance C (from the frequency of maximum f_{\max} of the imaginary part of impedance, Z'' , where $\omega_{\max}RC = 1$; $\omega_{\max} = 2\pi f_{\max}$ and $Z'' = -j\omega C$), and the depression angle α for the corresponding Z'' , Z' semicircle. The very high series resistance R_{ex} depends strongly on T but is practically independent of ΔE in the higher frequency region $f > 20$ kHz. Depression angles $\alpha < 15^\circ$ obtained for for the grain boundary semicircle (taken in air) are typical for the CGO electrolyte (3, 4, 7).

The values of activation energy, obtained from the $R_{\text{ex}}^{-1}, T^{-1}$ -plots (R_{ex} is the so-called very high frequency series resistance) for the grain boundary conductivities ($E_{\text{gb}} \approx 1.0$ eV), are in a reasonable agreement with those obtained elsewhere (4). The medium and low frequency arcs at $f < 20$ kHz characterise the overall performance of the cathode process and the so-called total polarisation resistance R_p can be obtained. The width of medium and low frequency arcs at fixed T and ΔE increases in the order Sys 1 < Sys 2 < Sys 3 (thus, with the atom mass of the A-site element in the perovskite cathode). At $T = \text{const.}$ and $f < 20$ kHz the total polarisation resistance of the overall cathode reaction R_p decreases with rising the negative polarisation, and at $\Delta E = \text{const.}$ R_p decreases with increasing temperature. The dependence of R_p on ΔE is more pronounced for Sys 3 and is smallest for Sys 1. The medium-frequency arc for Sys 1 and depression in the Z', Z'' -plots for Sys 2 and Sys 3 decrease with increasing temperature and disappears at $T > 873$ K. According to Refs. (3, 4) the surface exchange kinetics dominate at higher temperature. The arc attributed to the mass transfer of the oxygen anion in the cathode material is larger in the case of higher sintering temperature as well as for GSCO cathode, probably due to the changes in the microstructural characteristics (3). The characteristic relation time τ_{max} obtained from the low frequency part of the Z', Z'' -plots depends noticeably on the chemical composition and τ_{max} is shorter for GSCO compared with LSCO. τ_{max} depends on T and τ_{max} decreases with rising the thermal fluctuation energy. However, the characteristic frequency is practically independent of the cathode potential and, thus, the reaction mechanism, i.e. the nature of the prevailing process, is independent of ΔE .

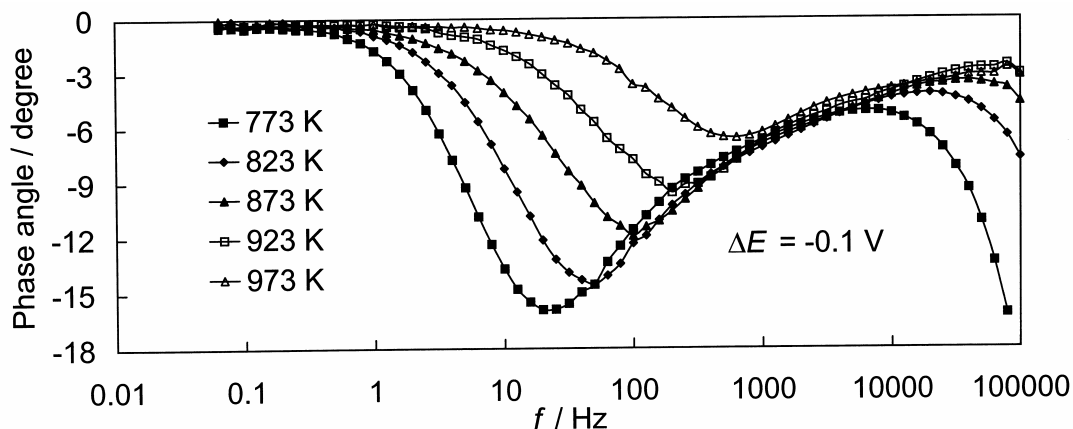


Figure 2. Phase angle vs. frequency plots for Sys 2 at various temperatures.

The influence of the cathode material and T on the electrochemical characteristics of the semicells is very well visible in Fig. 2, where the dependence of the phase angle (δ) on ac frequency is given. The data in Fig. 2 show that at $T \leq 773$ K there prevails mixed kinetics behaviour for Sys 2 and especially for Sys 3 (slow mass transfer (diffusion) and charge transfer steps). At higher negative potentials and temperatures the systems tend toward purely charge transfer limited mechanism ($\delta \geq -5^\circ$). However, the shape of $\delta, \log f$ plots shows that at $f \leq 20$ kHz for Sys 1 there are two very well separated processes with different time constants. For Sys 3 and Sys 2 there seems to be only one (or two, but not clearly separable) mainly diffusion-limited charge transfer process at $T \leq 773$ K. However, the noticeable dependence of δ on ΔE indicates the very complicated mass transfer process of the charged oxygen species in porous cathode for Sys 3.

Fitting of the complex impedance plane plots

The data in Fig. 1, to a first approximation, can be simulated with the chi-square function $\chi^2 \leq 6 \times 10^{-4}$ and weighted sum of squares $\Delta^2 < 0.1$ by the equivalent circuit (23, 24) presented in Fig. 1a, where R_{ex} is the total very high frequency series resistance of the system $R_{\text{ex}} \equiv Z_1(\omega \rightarrow \infty)$ (practically independent of ΔE); CPE_1 , R_1 , CPE_2 and R_2 are the so-called high-frequency and low-frequency constant phase element and charge transfer resistance values, respectively. $Z_{\text{CPE}} = A^{-1}(j\omega)^{-\alpha}$, where A is constant and α is fractional exponent. For fitting the Z'' , Z' -plots, the Zview 2.2 software has been used (24). Differently from the so-called mixed cathodes (LSCO + CGO) (3), for Sys 1, Sys 2 and Sys 3 there is no very well separable semicircles in the region of high frequencies because the so-called grain boundary resistance R_{gb} has very low values, indicating that the transfer of charged O^{2-} in the electrolyte as well as at the cathode | electrolyte phase boundary is quick. It should be noted that at higher T , differently from Sys 1, the shape of the Nyquist plots for Sys 2 and Sys 3 indicates that the equivalent circuit in Fig. 1a can be simplified and only the so-called low-frequency circuit, i.e. the low frequency process has mixed kinetics behaviour. The electrical double layer capacitance C_1 (medium-frequency circuit) has noticeable influence on the impedance characteristics (Z'') only at $T < 873$ K and $10 \text{ Hz} < f < 20 \text{ kHz}$.

A better fit of the Z'' , Z' -plots has been obtained by using the equivalent circuit in Fig. 1b, where the CPE_2 has been exchanged to the generalised finite length Warburg element (GFW) for a short circuit terminus model (Fig. 1b) expressed as

$$Z_{\text{GFW}} = \frac{R_{\text{D}} \tanh\left[(i\omega L^2 / D)^{\alpha_{\text{w}}}\right]}{(i\omega L^2 / D)^{\alpha_{\text{w}}}} \quad (1)$$

where R_{D} is the limiting diffusion (mass transfer) resistance, L is the effective diffusion layer thickness, D is the effective diffusion coefficient of a particle and α_{w} is a fractional exponent in the diffusion impedance expression (3, 23, 24). In agreement with Refs. (23, 24), the fractal exponent values $\alpha_2 \leq 0.5$ (obtained by using the equivalent circuit in Fig. 1a) for the low-frequency arc 2 in the case of systems investigated indicate that CPE_2 behaves as a Warburg-type diffusion impedance. The very small chi-square function values $\chi^2 < 2 \times 10^{-4}$ and weighted sum of squares $\Delta^2 < 0.03$ have been established. The relative residuals (23, 24) obtained for this circuit are very low and have a random distribution in the whole frequency region studied. Therefore it seems that the second arc at $T \leq 873$ K characterises the kinetically mixed, charge transfer and diffusion-like (mass transfer) limited adsorption processes ($|\delta| < 15^\circ$) as the values of α_{w} are somewhat lower than 0.5 (3). According to the results of simulations, R_{ex} decreases with rising temperature and in the order of systems Sys 3 > Sys 2 > Sys 1. The diffusion resistance R_{D} and the low-frequency charge transfer resistance R_2 decrease with increasing temperature and $|\Delta E|$ if $\Delta E \leq -0.2$ V and in the order of systems Sys 3 > Sys 2 > Sys 1. For all systems studied, there is a small maximum in the $R_{\text{D}}, \Delta E$ as well as $R_2, \Delta E$ dependences near $\Delta E = -0.1$ V. The high-frequency capacitance C_1 and adsorption capacitance C_2 increase with $|\Delta E|$ and in the order Sys 1 < Sys 2 < Sys 3, i.e. in the reverse order of R_{D} and R_2 . Very high values of C_2 have been established for Sys 1, Sys 2

and Sys 3 ($C_2 > 4 \times 10^{-3} \text{ F cm}^{-2}$), i.e. the accumulation of oxygen ions inside the porous cathode is possible. At fixed potential, the values of C_1 and C_2 decrease with rising temperature, i.e. with the rate of the cathodic reaction.

Activation energy, current relaxation plots and transfer coefficient

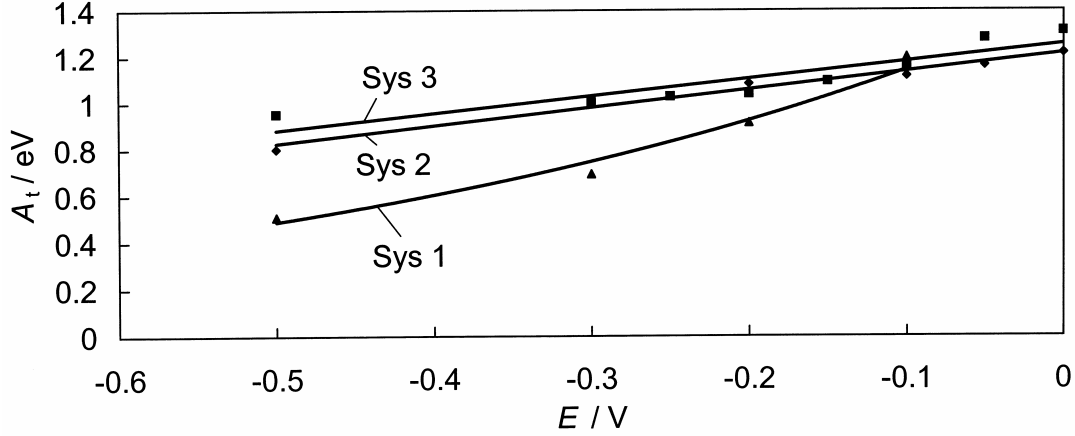


Figure 3. Total activation energy vs. electrode potential plots.

The capacitive parts of the impedance spectra at $f \leq 20 \text{ kHz}$ were used to determine the polarisation resistance (R_p) from the difference between the intercepts of the very low and high frequency parts of the spectra with the Z' -axis of Nyquist plots. R_p allows the quantification of the total potential loss of the overall cathodic (reduction) processes, taking into account the ohmic and activation polarisations, as well as the mass transport limitation. Comparison of the data shows that the total polarisation resistance increases in the order Sys 1 < Sys 2 < Sys 3. Including the high-frequency arc 1 and low-frequency arc 2, the total cathode polarisation resistance R_p is less than 0.2, 0.4 and 1.5 $\Omega \text{ cm}^2$ for Sys 1, Sys 2 and Sys 3, respectively, at $T = 973 \text{ K}$. Thus, noticeably higher R_p values have been obtained for Sys 3. As shown before, this is mainly caused by the very high diffusion impedance (mass transfer resistance) values for Sys 3, compared with Sys 1. On the other hand, the fitting data at fixed ΔE can be used for obtaining the polarisation resistance values for the medium-frequency process (arc 1), R_{p1} , and low-frequency process, R_{p2} . Therefore, the R_p , R_{p1} and R_{p2} have been used for the calculation of the values for total cathode reaction conductivity σ_t (obtained from total R_p), medium-frequency region conductivity σ_1 (obtained from R_{p1}), and low-frequency conductivity σ_2 values (obtained from R_{p2}). The linear dependences of Arrhenius plots have been used for the calculation of the values of activation energy, given in Fig. 3. The value of A_t obtained at $\Delta E = 0$ is independent of the cathode studied, but the values of A_t , A_1 and A_2 for Sys 1 decrease very rapidly with increasing the negative potential. The value of $A_t = 1.24 \text{ eV}$ obtained for Sys 1 and Sys 2 at zero potential is in a reasonable agreement with the data obtained in Refs. (3, 4) ($A_t = 1.04 \text{ eV}$). The value of activation energy for Sys 3, obtained from Z' , Z'' -plots, is in a reasonable agreement with the value of A_D , obtained from the R_p , T -plots. Thus, for Sys 3 the arc 2 at lower T characterises mainly the mass transfer (i.e. diffusion-like) limited process of the electrochemically active oxygen pieces.

Chronoamperometry curves obtained indicate that the shape of the i_c, t -curves depends on T , ΔE and cathode composition. At small times ($t < 2.0$ s) $|i_c|$ increases with time for materials studied. The stable $|i_c|$ values have been established at $T \leq 773$ K in the case of $t > 5.0$ s, but at $T \geq 973$ K at very short charging times $t < 1$ s. At lower temperatures ($T \leq 773$ K) the cathodic current density values are noticeably higher for Sys 1 than for Sys 3, indicating that the rate of cathodic reaction increases in the order Sys 3 < Sys 2 < Sys 1. The increase in the cathode current density with time can be explained by extending the active reaction zone from the open surface area to the porous surface of mixed conducting cathode. The increase in concentration of the “charged oxygen” species with increasing the negative cathode potential will improve the catalytic activity of the cathode and the decrease in the values of A_t . However, the fitting data of the Z', Z'' -plots show that the oxygen reduction in Sys 3 and Sys 2 is mainly limited by the mixed kinetics, i.e. charge transfer and diffusion-like steps, in the porous cathode material when the cathodic potential is applied to the interface.

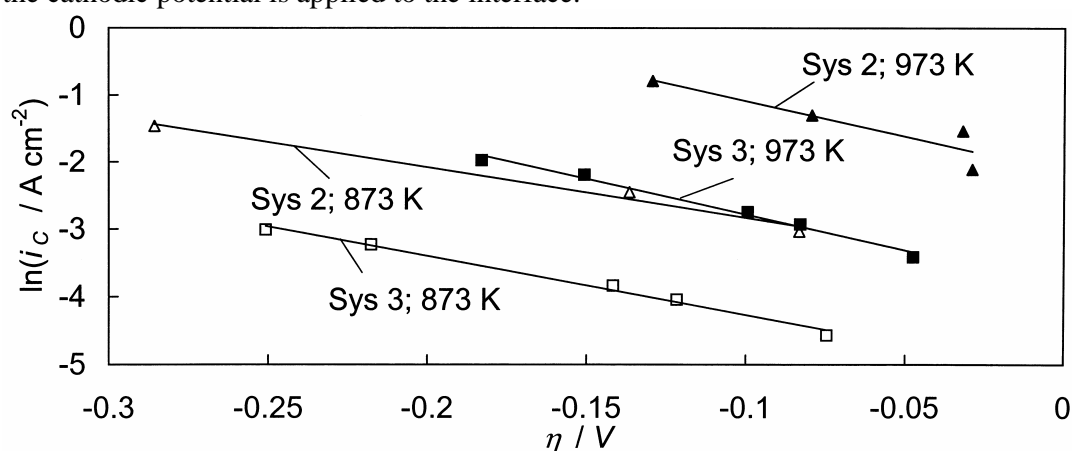


Figure 4. Current density vs. overpotential dependences for Sys2 and Sys 3 at various temperatures.

The Tafel-like overpotential $\eta, \ln i_c$ -curves, calculated from the i_c, t -curves at $t > 10$ s when the stable values of i_c have been established at fixed ΔE and T , are presented in Fig. 4. (ΔE values have been corrected by the ohmic potential drop to obtain η). According to the calculations for Sys 1 and Sys 3 the values of transfer coefficient, α_c , somewhat higher than 0.5 indicate the mixed kinetic mechanism, i.e. slow O_{ads}^- or O_{ads} diffusion, in addition to slow electron transfer seems to be the rate-determining step. The value of α_c near 0.5 for Sys 2 indicates the charge transfer limited mechanism. The values of α_c for the systems studied increase slightly with rising temperature. The exchange current density (i_0), obtained from the Tafel plots, increases with temperature and in the order of systems Sys 3 < Sys 2 < Sys 1.

Influence of operation time on the electrochemical characteristics of half-cells

Fig. 5 shows the complex impedance plane plots for Sys 2 at different operation times. The similar dependences have been obtained at different fixed polarisations for other half-cells too. (At least 30 thermal cycles have been made with Sys 1, and 5 thermal cycles with Sys 2 and Sys 3.) According to the experimental results at higher temperature

($T \geq 873$ K), the shape of the Z'' , Z' -plots is practically independent of operation time during about 1200 hours for Sys 2 and during 4600 hours for Sys 1. It should be noted that at short working time (from 100 to 200 h) the small decrease in R_{ex} and increase in R_p have been observed, but at $t > 200$ h the stabilisation of the electrochemical parameters has been established. The high-frequency series resistance values $Z'(\omega \rightarrow \infty) = R_{ex}$ for all systems studied do not depend practically on the operation time more than 200 hours. At lower temperature, the small increase of low-frequency polarisation resistance (R_p) has been established for Sys 2. The time stability of R_p is somewhat higher for Sys 1 compared with Sys 2. The results of fitting the Z'' , Z' -plots shows that the diffusion resistance R_D , charge transfer resistance R_2 , adsorption capacitance C_2 and fractional exponent of diffusion impedance α_w are practically independent of operation time if $T \geq 823$ K. At $T \leq 773$ K, only the small decrease of R_D and α_w for Sys 1, and more pronounced increase of R_D for Sys 2 is possible. The values of R_2 obtained are practically independent of operation time if $T \geq 823$ K, and only at $T \leq 773$ K, R_2 very weakly increases with time (up to ~20%).

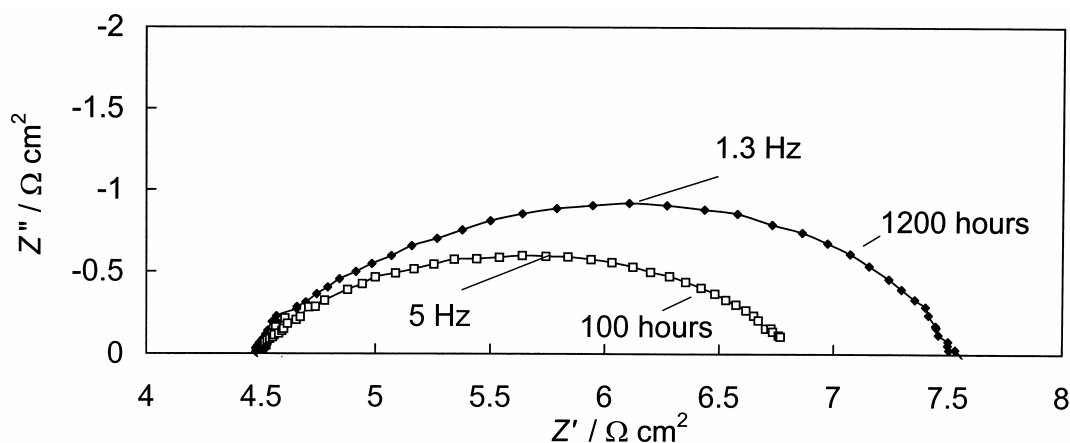


Fig. 5. Time dependence of the Nyquist plots for $\text{Pr}_{0.6}\text{Sr}_{0.4}\text{CoO}_{3.8}$ at $\Delta E = -0.1$ V and $T = 873$ K.

The Arrhenius-like and Tafel-like plots have been constructed at different operation times. At $|\Delta E| > 0.1$ V, the activation energy only very slightly decreases with operation time. The exchange current density i_0 increases (10...20%) with operation time at lower polarisations, but this dependence is small at $|\Delta E| \geq 0.2$ V. The transfer coefficient α_c for oxygen reduction is practically independent of the operation time.

CONCLUSIONS

The kinetically mixed process (slow mass transport and electron transfer stages) seems to take place for all systems studied in air at $773 \leq T \leq 1073$ K. The values of activation energy, decreasing with the increasingly negative cathode potential, and of the transfer coefficient $\alpha_c > 0.5$ indicate that in addition to the electron transfer process (reduction of oxygen) the mass transfer process of electrochemically active species in solid cathode material or at the internal porous cathode surface can probably be the rate-determining steps in agreement with the fitting results of the Nyquist plots. The operation time

stability test shows that these half-cells can be used for the future development of solid oxide fuel cells, working in the medium temperature range.

ACKNOWLEDGEMENTS

This work is supported by AS Elcogen under the grants LFKFE 01081 and LFKFE 03006.

REFERENCES

1. S. C. Singhal, *Solid State Ionics* **135**, 305 (2000).
2. A. Weber, E. Ivers-Tiffée, *J. Power Sources* **127**, 273 (2004).
3. E. Lust, G. Nurk, S. Kallip, I. Kivi, P. Möller, Electrochemical characteristics of $\text{Ce}_{0.8}\text{Gd}_{0.2}\text{O}_{1.9} \mid \text{La}_{0.6}\text{Sr}_{0.4}\text{CoO}_{3-\delta} + \text{Ce}_{0.8}\text{Gd}_{0.2}\text{O}_{1.9}$ half-cell, *J. Solid State Electrochem.* (accepted).
4. V. Dusastre, A. Kilner, *Solid State Ionics* **126**, 163 (1999).
5. S. P. Jiang, *Solid State Ionics* **146**, 1 (2002).
6. M. Mogensen, N. M. Sammes, G. A. Tompsett, *Solid State Ionics* **129**, 63 (2000).
7. S.B. Adler, *Solid State Ionics* **111**, 125 (1998).
8. M. Gödickemeier, L.J. Gauckler, *J. Electrochem. Soc.* **145**, 414 (1998).
9. C.S. Tedmon, H.S. Spacil, S.P. Mitoff, *J. Electrochem. Soc.* **116**, 1170 (1969).
10. O. Yamamoto, Y. Takeda, R. Kanno, M. Noda, *Solid State Ionics* **22**, 241 (1987).
11. Y. Teraoka, H. Zhang, S. Furukawa, N. Yamazoe, *Chem. Lett* **14**, 1743 (1985).
12. H. Arai, T. Yamada, K. Egachi, T. Seigama, *Appl. Catal.* **26**, 394 (1986).
13. A. Esquirol, N.P. Brandon, J.A. Kilner, M. Mogensen, *J. Electrochem. Soc.* **151**, 1847 (2004).
14. J.N. Eastabook, *Philos. Mag. (Eight Sek.)* **2**, 1421 (1957).
15. G.Ch. Klostogbudis, N. Vasilakos, Ch. Ftikos, *Solid State Ionics* **106**, 207 (1998).
16. J.B. Goodenough, *J. Phys. Chem. Solids* **6**, 287 (1958).
17. P.M. Raccah, J.B. Goodenough, *Phys. Rev.* **155**, 932 (1967).
18. V.G. Bhide, D.S. Rajoria, G. Rama Rao, C.N.R. Rao, *Phys. Rev. B* **6**, 1021 (1972).
19. J.M. Ralph, C. Rossignol, R. Kumar, *J. Electrochem. Soc.* **150**, A 1518 (2003).
20. C. Rossignol, J.M. Ralph, J.-M. Bae, J.T. Vaughey, *Solid State Ionics* **175**, 59 (2004).
21. Y. Takeda, H. Ueno, N. Imanishi, O. Yamamoto, N. Sammes, M.B. Phillips, *Solid State Ionics* **86-88**, 1187 (1996).
22. M.B. Phillips, N.M. Sammes, O. Yamamoto, *Solid State Ionics* **123**, 131 (1999).
23. J. R. MacDonald, Editor, *Impedance Spectroscopy: Emphasisizing Solid Materials and Systems*, Wiley, New York, (1987).
24. J. R. MacDonald, ZPLOT for Windows (Version 2.2) fitting program, LEVM 6.0.